

DISTREAL: Distributed Resource-Aware Learning in Heterogeneous Systems

Martin Rapp¹, Ramin Khalili², Kilian Pfeiffer¹, Jörg Henkel¹

¹ Karlsruhe Institute of Technology, Karlsruhe, Germany

² Huawei Research Center, Munich, Germany

martin.rapp@kit.edu, ramin.khalili@huawei.com, kilian.pfeiffer@kit.edu, henkel@kit.edu

Abstract

We study the problem of distributed training of neural networks (NNs) on devices with heterogeneous, limited, and time-varying availability of computational resources. We present an adaptive, resource-aware, on-device learning mechanism, *DISTREAL*, which is able to fully and efficiently utilize the available resources on devices in a distributed manner, increasing the convergence speed. This is achieved with a dropout mechanism that dynamically adjusts the computational complexity of training an NN by randomly dropping filters of convolutional layers of the model. Our main contribution is the introduction of a design space exploration (DSE) technique, which finds Pareto-optimal per-layer dropout vectors with respect to resource requirements and convergence speed of the training. Applying this technique, each device is able to dynamically select the dropout vector that fits its available resource without requiring any assistance from the server. We implement our solution in a federated learning (FL) system, where the availability of computational resources varies both between devices and over time, and show through extensive evaluation that we are able to significantly increase the convergence speed over the state of the art without compromising on the final accuracy.

Introduction

Deep learning has achieved impressive results in a number of diverse domains, such as image classification (Howard et al. 2017; Tan and Le 2019), board and video games (Silver et al. 2016; Mnih et al. 2016), and is widely applied to distributed systems, such as mobile and sensor networks (Zhang, Patras, and Haddadi 2019), as we consider in this paper. Centralized deep learning techniques, where the training is performed in a single location (e.g., a data center), is often costly, as data would need to be collected and sent all over the network to that centralized entity (Shi et al. 2020), and might not be feasible/authorized if the training uses users' private data. FL (McMahan et al. 2017) emerged as an alternative to such techniques, performing distributed learning on each device with the locally available data.

FL has proven effective in large-scale systems (Bonawitz et al. 2019; Liu, Wang, and Liu 2019; Chen et al. 2020b). However, training of a deep NN model is resource-hungry

in terms of computation, energy, time, etc. (You et al. 2018), and it is rather unrealistic to assume that all devices in an FL system can perform all types of training computations all the time, especially if the training is distributed on edge devices, e.g., as suggested for 6G systems.¹ This is as the computational capabilities of devices participating in an FL system may be heterogeneous, e.g., different hardware, different generations (Bonawitz et al. 2019). *More importantly, the resources available on a device for training could change over time.* This could for instance be due to shared resource contention (Dhar et al. 2019), where CPU time, cache memory, energy, etc. are shared between the learning and parallel tasks. We illustrate this with the following two examples.

1) Edge computing has been employed in ML-based real-time video analytics, where each edge device processes images from several camera modules (Anathanarayanan et al. 2017). Currently, edge devices mostly perform inference, but there is a clear trend towards additionally performing distributed learning via FL (Zhou et al. 2019). The learning task shares computational resources with the inference tasks. The inference workload depends on the activity in the video images and changes over time, as processing is skipped for subsequent similar images to save resources (Anathanarayanan et al. 2017). These changes happen fast, i.e., in the order of seconds (Zhang et al. 2017), while FL round times may be minutes (Bonawitz et al. 2019). 2) Google *GBoard* (Yang et al. 2018) trains a next-word-prediction model using FL on end users' mobile phones. To avoid slowing down user applications, and thereby degrading the user experience, training is performed only when the device is charging and idle, and aborted when these conditions change. This introduces a bias towards certain devices and users, degrading the model accuracy (Yang et al. 2018). This can be resolved by allowing training also when the device is in use, but only using free resources. Smartphone workloads change within seconds (Tu et al. 2014), which is faster than the *GBoard* round time of several minutes. In both examples, the learning task is subject to fast-changing resource availability.

While several works study the problem of heterogeneity across devices (Li et al. 2020a; Imteaj et al. 2020), time-

¹EU's Horizon Europe (European Commission 2021a,b) calls for proposals, as well as 5GIA (5G Infrastructure Association) and SRIA (Strategic Research and Innovation Agenda) reports (Bernardos and Uusitalo 2021; NetWorld 2020) detail such a vision.

varying resource availability has so far been neglected. In this paper, we propose a distributed, resource-aware, adaptive, on-device learning technique, *DISTREAL*, which enables us to fully exploit and efficiently utilize available resources on devices for the training, dealing with all these types of heterogeneity. Our objective is to maximize the accuracy that is reached after limited training time on devices, i.e., convergence speed. To fulfill this goal, we should make sure that C1) The available resources on a device are *fully* exploited. This requires fine-grained adjustability of the training model on a device, and a method to instantly react to changes; and C2) The available, limited, resources on a device are used *efficiently*, to maximize the accuracy improvement and hence the overall convergence speed. Specifically, we provide the following novel contributions:

- We introduce and formulate the problem of heterogeneous time-varying resource availability in FL.
- We propose a dropout technique to adjust the computational complexity (resource requirements) of training the model *at any time*. Thereby, each device locally decides the dropout setting which fits its available resources, without requiring any assistance from the server, addressing C1. This is different from the state-of-the-art techniques, such as (Caldas et al. 2018; Horváth et al. 2021; Xu et al. 2019; Diao, Ding, and Tarokh 2021), where the server is responsible for regulating resource requirements of training for each device at the beginning of each training round, which may take several minutes.
- We show that using different per-layer dropout rates achieves a much better trade-off between the resource requirements and the convergence speed, compared to using the same rate at all layers as the state of the art (Caldas et al. 2018; Diao, Ding, and Tarokh 2021), addressing C2. We present a DSE technique to automatically find the Pareto-optimal dropout vectors at design time.

We implement our solution *DISTREAL* in an FL system, in which the availability of computational resources varies both between devices and over time. We show through extensive evaluation that *DISTREAL* significantly increases the convergence speed over the state of the art, and is robust to the rapid changes in resource availability at devices, without compromising on the final accuracy.

System Model and Problem Definition

System Model We target a distributed system, which comprises one *server* and N distributed *devices* that act as clients. Each device i holds its own local training data X_i . The system uses FL for decentralized training of an NN model from the distributed data. We target a synchronous coordination scheme, which divides the training into many *rounds*. At the beginning of a round, the server selects n devices to participate in the training. Each selected device downloads the recent model from the server, trains it with its local data, and sends weight updates back to the server. The server combines all received weight updates to a single update by weighted averaging. Updates from devices that take too long to perform the training (stragglers) are discarded.

Device Resource Model The devices are subject to time-varying limited computational resource availability for training. To which degree the availability of a certain resource affects the training time of an NN depends on the NN and hyperparameters, but also on the deep learning library implementation and the underlying hardware (Chen et al. 2020c). We abstract from such specifics of the hardware and software implementation, and from the constrained physical resource to keep this work applicable to many systems by representing the resource availability in the number of multiply-accumulate operations (MACs) that a device can calculate per time given its specifications and available resources. MAC operations are the fundamental building block of NNs (e.g., fully-connected and convolutional layers) and account for the great majority of operations (Krizhevsky, Sutskever, and Hinton 2012). In the appendix, we also provide experimental evidence for the suitability of MACs/s as an abstract metric. Resource availability varies between devices and over time. Therefore, these resource availabilities $r_i(t)$ depend on the device i , and the current time t . Resources may change at any time, i.e., also within an FL round. Resources are not required to be known ahead of time.

Objective Our objective is to maximize the convergence speed of training, i.e., the reached accuracy after a number of rounds, under heterogeneous (between devices and over time) resource availability.

Related Work

Many works on resource-aware machine learning focus on resource-aware *inference* (Tann et al. 2016; Yu et al. 2018; Amir and Givargis 2018; Li et al. 2021a). These techniques allow adapting the inference to dynamically changing availability of resources at run time but are not applicable to training. Resource-aware *training* is recently getting increasing attention, mostly in the context of FL. Most attention has so far been paid to limited *communication* resources, leading to solutions, such as compression, quantization, and sketching (Shi et al. 2020; Thakker et al. 2019). Importantly, these works do not reduce the *computational* resources for training, as they are applied after local training has finished. These works are complementary/orthogonal to our work and can be adopted to our solution (see the section on the run-time technique). Techniques on computation-resource-aware training can be categorized into two classes: techniques that always train the full NN on each device but with fewer data/relaxed timing and techniques that train subsets of the NN.

Train Full NNs FedProx (Li et al. 2020b) allows devices participating in an FL system to deliver partial results to the server by dropping training examples that could not be processed with the available resources. Our previous work (Rapp, Khalili, and Henkel 2020) studied multi-head networks where each device uses the head that fits its available resources. Devices only synchronize the weights of the first shared layers. However, this technique has low adaptability as only a few resource levels can be supported. Asynchronous variants of FL have been proposed that allow devices to finish training at any time (Chen et al. 2020a; Xie,

Koyejo, and Gupta 2020). However, asynchronous synchronization may reduce the convergence stability (McMahan et al. 2017; Xu et al. 2019). Techniques based on Federated Distillation (Li and Wang 2019; Chang et al. 2019; Lin et al. 2020) synchronize knowledge between devices by exchanging labels on a public dataset instead of exchanging NN weights. Therefore, each device has the design flexibility to use an NN model according to its constraints. However, Federated Distillation cannot cope with time-varying resources.

Train NN Subsets Several techniques perform training only on a dynamic subset of the NN, to be able to fit the resource requirements of training to the resource availability on each device. FjORD (Horváth et al. 2021), Yu and Li (2021), and HeteroFL (Diao, Ding, and Tarokh 2021) select subsets of the NN for each device at the beginning of each round. They select the subsets in a hierarchical way, where smaller subsets are fully contained in larger subsets. HeteroFL introduces a shrinkage ratio s that defines the ratio of removed hidden channels to reduce the resource requirements of the NN. The same parameter s is applied repeatedly to all layers to obtain several subsets with decreasing resource requirements. Using hierarchical subsets restricts the granularity of resource requirements, as increasing the number of supported subsets reduces the achievable accuracy (Tann et al. 2016). This limitation can be avoided by selecting subsets randomly, i.e., use different subsets in every round. ELFISH (Xu et al. 2019) randomly removes neurons before training on slow devices at the beginning of a round. Graham, Reizenstein, and Robinson (2015) study the suitability of dropout (Srivastava et al. 2014) to reduce resource requirements. They find that computations can only be saved if dropout is done in a structured way, i.e., the same neurons are dropped for all samples of a mini-batch. Federated Dropout (Caldas et al. 2018) has been originally proposed to reduce the communication and computation overhead of FL. They perform dropout at the server and train a repacked smaller network on the devices. The dropout masks are changed randomly in each round, which results in all parts of the NN being trained eventually. However, they use the same dropout rate for all devices and a single dropout rate for all layers. All these works select the trained subset at the server, which may reduce the communication volume, but importantly does not allow to adapt to changing resource availability on the devices within a round.

Resource-Aware Training of NNs

Our technique comprises two parts. At run time (online), we dynamically drop parts of the NN using an adapted version of dropout (Srivastava et al. 2014). The Pareto-optimal vectors of dropout rates w.r.t. convergence speed and resource requirements are obtained at design time (offline) using a DSE. Before going into the details of our contribution, we introduce dropout as the basis of our technique.

Dropout to Reduce Computations In Training Dropout was originally designed as a regularization method to mitigate overfitting (Srivastava et al. 2014). It randomly drops individual neurons during training with a certain probability

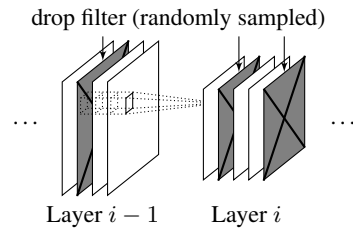


Figure 1: Filter-based structured dropout in a convolutional layer maintains regularity in the calculations while significantly reducing the required computations.

(dropout rate). This results in an irregular fine-grained pattern of dropped neurons. All major deep learning libraries perform dropout by calculating the output of all neurons and multiplying the dropped ones with 0 (Abadi et al. 2015; Paszke et al. 2019). This wastes computational resources; it would be more efficient to not calculate values that are going to be dropped. However, convolutional and fully-connected layers are implemented as matrix-vector or matrix-matrix operations that are heavily optimized with the help of vectorization (Abadi et al. 2015; Paszke et al. 2019). Skipping the calculation of individual values results in sparse matrix operations, which breaks vectorization, increasing the required resources instead of decreasing them (Song et al. 2019).

To reduce the number of computations, the dropout pattern needs to show some regularity that still allows using vectorization of dense matrix operations. This can be achieved by dropping contiguous parts of the computation (Graham, Reizenstein, and Robinson 2015). Modern NNs consist of many different layer types such as convolutional, pooling, fully-connected, activation, or normalization layers. Many of these layers are computationally lightweight (e.g., pooling), while some contain the majority of computations (convolutional and fully-connected layers). In state-of-the-art convolutional NNs, the convolutional part requires orders of magnitude more MACs than the fully-connected part. (See the appendix for an experimental analysis.) We, therefore, argue that a technique to save computations needs to target convolutional layers. Fig. 1 depicts filter-based structured dropout in a convolutional layer, as we apply in this paper: instead of dropping individual pixels in the output, whole filters are dropped stochastically. This approach reduces the number of computations while allowing to keep existing vectorization methods.

Fig. 2 depicts how the number of MACs of the forward pass evolves when we apply different vectors of per-layer dropouts for DenseNet-40 (details in the experimental evaluation). We apply the DSE technique introduced in this paper to determine these vectors and show in the x-axis the resulting ratio of dropped filters². We observe that the number of MACs decreases almost quadratically with this ratio. We also report the training time of a single mini-batch on a Raspberry Pi 4, which serves as an example for an IoT de-

²Multiple vectors may result in the same ratio of dropped filters, while providing different convergence / resource requirement trade-offs, explaining why for some ratios we have multiple MACs.

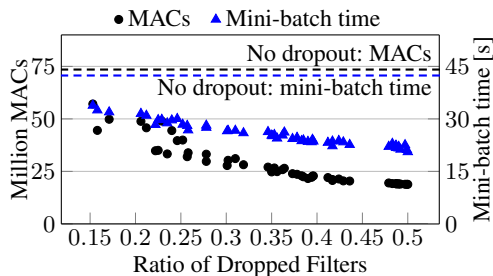


Figure 2: The number of MACs and mini-batch training time decrease quadratically with the ratio of dropped filters.

vice, using an implementation of this structured dropout in PyTorch (Paszke et al. 2019), which is publicly available³. A training step (forward pass, backpropagation, and weight updates) requires about $\sim 2\times$ more MACs than the forward pass alone (Amodei et al. 2018). The mini-batch training time shows a similar trend as the number of MACs but with an offset. This is because our implementation does not modify the backend of PyTorch to be aware of this dropout, which results in copy operations of weight tensors to repack them. As a consequence, the measured benefits are smaller than what is theoretically achievable. Changing the backend would get the benefits closer to the optimum but is not easily doable because of closed sources (e.g., of CUDA). In summary, this experiment shows that structured dropout significantly reduces the required computational resources.

The dropout rates also change the convergence speed. A higher dropout rate in a layer means that in each training update, a smaller fraction of the layer’s weights is updated, thereby slowing down the training. As a consequence, the dropout rate determines a trade-off between the resource requirements and the convergence speed. The dropout rate should always be selected as low as the available resources allow. To cope with changing resource availability, we propose to *dynamically change the dropout rate at run time*. Inference uses always the whole model.

Design-Time DSE: Find Pareto-Optimal Dropout Vectors The resource requirements (MACs) and convergence speed both depend on the dropout rates of *each layer*. Prior works restrict themselves to choosing a common dropout rate for all layers (Caldas et al. 2018). Relaxing this restriction opens up a larger design space, where each dropout rate of each layer is adjusted towards a better trade-off between resource requirements and training convergence. However, this design space could be too large to be explored manually. For example, DenseNet-100 has 99 convolutional layers that each need to be assigned a dropout rate. Some works apply simple parametric functions of the depth to similar problems (Huang et al. 2016). However, this only works in case of a homogeneous NN structure, where properties of layers (e.g., MACs) change monotonically. For instance, DenseNet layers alternate between computationally lightweight and complex, rendering a simple parametric function sub-optimal.

³<https://git.scc.kit.edu/CES/DISTREAL>

This section describes the required automated DSE technique to efficiently explore such a large space. The DSE is executed only once at design time (offline).

Specifically, the design space contains all combinations of dropout values per layer. We select dropout values from the continuous range $[0, 0.5]$ because higher values reduce the final achievable accuracy, as we observe in our experiments, as well as indicated in previous studies (Srivastava et al. 2014). For an NN with k convolutional layers, the design space is $[0, 0.5]^k$. We have two objectives, the resource requirements and the convergence speed.

Resource Requirements: As discussed in the device resource model, the number of MACs is an implementation-independent representation of the resource requirements. Dropout is a probabilistic process, i.e., the number of MACs varies between different update steps. The resource requirements with a certain dropout vector is represented by the expectation value of the number of MACs of the forward pass. This number can be analytically computed depending on the layer topology, the dropout rate of this layer and preceding layers. The appendix lists equations for different layer types.

Convergence Speed: The convergence speed with a certain dropout vector is measured by observing the accuracy change when training. Exploring the search space takes too long if a full training with every candidate dropout vector is performed. Instead, we assess the accuracy change after a short training, similar to learning curve extrapolation in neural architecture search (Baker et al. 2017). We train for 64 mini-batches with batch size 64, which allows us to explore many candidate dropout vectors in a reasonable time. This corresponds to the amount of data collected by very few devices. To reduce the impact of random initialization, the NN is not trained from scratch but from a snapshot after partially training it on a distorted version of the dataset. For instance, we reduced the brightness, contrast, and saturation to 0.5 of the original value for CIFAR-10/100 datasets. The DSE, therefore, does not require access to the devices’ data, but only access to a small amount of similar (or even synthetic) data. To further reduce the impact of random variations, we repeat this with three different random seeds. The convergence speed is represented by the average accuracy improvement.

Fig. 3 shows our DSE flow. The problem of finding Pareto-optimal dropout vectors is a multi-objective optimization. This is a well-studied class of problems with many established algorithms. Evolutionary algorithms have successfully been employed for neural architecture search (Elsken, Metzen, and Hutter 2019), which is related to the problem studied in this section. Note that we are not searching for an architecture, but tune parameters of a given architecture. The output of the DSE is the Pareto-front of dropout vectors. To have a large variety of options to choose from at run time, but also keep a low number of vectors to be stored, the Pareto-front should be approximately equidistantly represented. We use the NSGA-II (Deb et al. 2002) genetic algorithm from the pygmo2 library (Biscani and Izzo 2020). NSGA-II explores the search space by crossover (combining parts of two dropout vectors) and mutation (random changes) of good dropout vec-

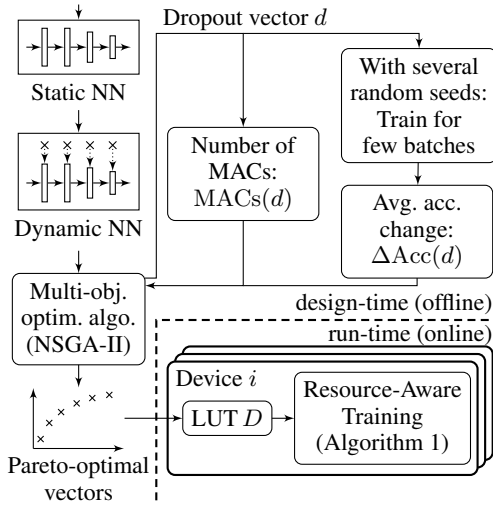


Figure 3: Efficient resource-aware training comprises the DSE to find Pareto-optimal vectors of dropout rates per layer and resource-aware training on each device at run time.

tors w.r.t. the objective function, and is designed to obtain dropout vectors that are equidistantly distributed across the Pareto-front. Thereby, an *individual* is one dropout vector containing the per-layer dropout rates. For our largest studied NN, DenseNet-100, this is 99 float values between 0 and 0.5. A *population* is a set of individuals. We use a population size of 64. A *generation* performs one optimization step on the population with the goal to find the Pareto-front. The optimization minimizes the following two-dimensional *fitness* function $f(d)$ for a dropout vector d , which normalizes the values of the resource requirements $\text{MACs}(d)$ and convergence speed $\Delta\text{Acc}(d)$ to the range $[0, 1]$:

$$f(d) = \left(\frac{\text{MACs}(d) - \text{MACs}(\{0.5, \dots, 0.5\})}{\text{MACs}(\{0, \dots, 0\}) - \text{MACs}(\{0.5, \dots, 0.5\})} \right) \left(\frac{\Delta\text{Acc}(\{0, \dots, 0\}) - \Delta\text{Acc}(d)}{\Delta\text{Acc}(\{0, \dots, 0\}) - \Delta\text{Acc}(\{0.5, \dots, 0.5\})} \right) \quad (1)$$

Fig. 4 shows the evolving population of dropout vectors for DenseNet-40. The initial population comprises random dropout vectors. We add two samples to the initial population (all dropout values are 0 / 0.5) to accelerate the exploration of the Pareto-front (leverage the crossover operation). After 50 generations of NSGA-II, the Pareto-front has fully evolved and shows a continuous trade-off between resource requirements and convergence speed. Importantly, the Pareto-front found by DSE provides a significantly better trade-off between resource requirements and convergence speed compared to using the same dropout rate for all layers.

Run Time: Resource-Aware Training of NNs After finding the Pareto-optimal dropout vectors, they are stored in a lookup table (LUT) D , along with the corresponding number of MACs. The LUT is small in size (e.g., 25 kB for DenseNet-100 for storing 64 dropout vector of 99 dropout values and the number of MACs, each in 32-bit format) and stays constant for all rounds. At run time, a device selects the dropout vector d that best corresponds to its resource

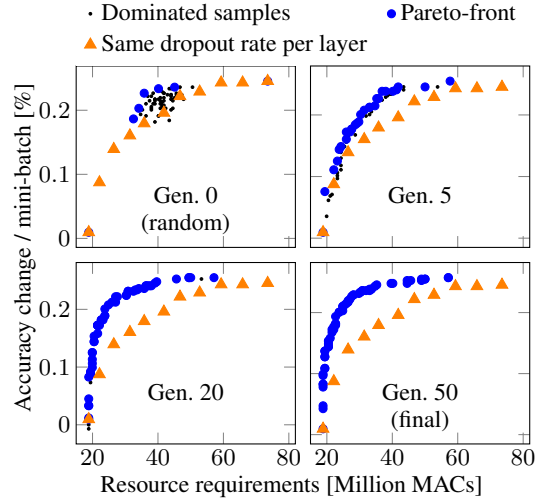


Figure 4: The evolving Pareto-front for DenseNet-40 significantly outperforms setting the same rate for all layers.

Algorithm 1: Each Selected Device i (Client)

Require: D : LUT of Pareto-optimal dropout vectors (from DSE)
receive θ_{init} from server
 $\theta \leftarrow \theta_{init}, c \leftarrow 0$
for each $b \in X_i$ **do** \triangleright iterate over mini-batches from local data
 $r \leftarrow r_i(t)$ \triangleright current resource availability
 $d \leftarrow D[r]$ \triangleright resource-aware dropout vector
Update dropout values of local NN with d
 $\theta \leftarrow \theta - \eta \frac{\partial}{\partial \theta} L(b; \theta)$ \triangleright update step
 $c \leftarrow c + \text{MACs}(d)$ \triangleright accumulate computations
send $(\theta - \theta_{init}, c)$ to server \triangleright weight update and computations

availability. If resource availability changes at the device, the dropout vectors can be adjusted to these changes at almost zero overhead before every mini-batch. No weight copies, recompilation, repacking of weights, etc. are required for adapting the resource requirements.

In an FL setting, each device selects its dropout vector at run time according to its resource availability, as shown in Algorithm 1. This is done at the granularity of single mini-batches, i.e., devices can quickly react to changes. Additionally, the server does not need to know the resource availability at each device at the beginning of the round, reducing signaling overhead, and avoiding the requirement to know resource availability ahead of time. This is important to maintain scalability with the number of devices. At the end of each round, the devices report back the weight updates and the computational resources they put into training (number of MACs, as stored in the LUT). The server (Algorithm 2) performs a weighted averaging of the received updates w.r.t. the devices' reported computational resources. Thereby, updates from devices that have trained with lower dropout rates, are weighted stronger. This is an extension of *FedAvg* (McMahan et al. 2017), which performs weighted averaging only based on the number of mini-batches. In the case of constant and same resource availability on all de-

Algorithm 2: Server

$\theta_0 \leftarrow$ random initialization
for each round $t = 1, 2, \dots$ **do**
 $K \leftarrow$ select n devices
 broadcast θ_{t-1} to selected devices K
 receive $(d\theta_i, c_i)$ from devices $i \in K$
 $C \leftarrow \sum_{i \in K} c_i$ \triangleright *tot. computations*
 $d\Theta \leftarrow \sum_{i \in K} c_i \cdot d\theta_i$ \triangleright *weighted sum*
 $d\theta \leftarrow d\Theta / C$ \triangleright *weighted average*
 $\theta_t \leftarrow \theta_{t-1} + d\theta$

	FEMNIST	CIFAR-10	CIFAR-100
#Devices	3,550	100	100
#Samples/device	181±70.7	500	500
Devices/round	35	10	10
Resources var.	3×	4×	4×

Table 1: System configuration for FL.

vices, our coordination technique behaves the same as *FedAvg*. As we do not change the type of data exchanged between the devices and the server, compared to *FedAvg*, we can still apply and adopt techniques that mitigate communication aspects, such as compression and sketched updates (Shi et al. 2020).

Experimental Results

This section demonstrates the benefits of *DISTREAL* with heterogeneous resource availability in an FL system.

Experimental Setup We study synchronous FL as described in the system model. We report the classification accuracy of the synchronized model at the end of each round. Our main performance metric is the *convergence speed*, i.e., the accuracy achieved after a certain number of rounds, but we also report the final accuracy after convergence.

The three datasets used in our experiments are *Federated Extended MNIST* (FEMNIST) (Cohen et al. 2017) with non-independently and identically distributed (non-iid) split data, similar to LEAF (Caldas et al. 2019), and CIFAR-10/100 (Krizhevsky and Hinton 2009). FEMNIST consists of 641,828 training and 160,129 test examples, each a 28×28 grayscale image of one out of 62 classes (10 digits, 26 upper- and 26 lower-case letters). CIFAR-10 consists of 50,000 training and 10,000 test examples, each a 32×32 RGB image of one out of 10 classes such as airplane or frogs. CIFAR-100 is similar to CIFAR-10 but uses 100 classes. Table 1 summarizes the configurations.

For FEMNIST, we use a similar network as used in Federated Dropout (Caldas et al. 2018), with a depth of 4 layers, requiring 4.0 million MACs in the forward pass. We use DenseNet (Huang et al. 2017) for CIFAR-10 and CIFAR-100 with growth rate $k = 12$ and depth of 40 and 100, respectively. This results in 74 million MACs for CIFAR-10 and 291 million MACs for CIFAR-100 in the forward pass. The DSE for these NNs takes around 15, 270, and 330 compute-hours, respectively, on a system with an Intel Core

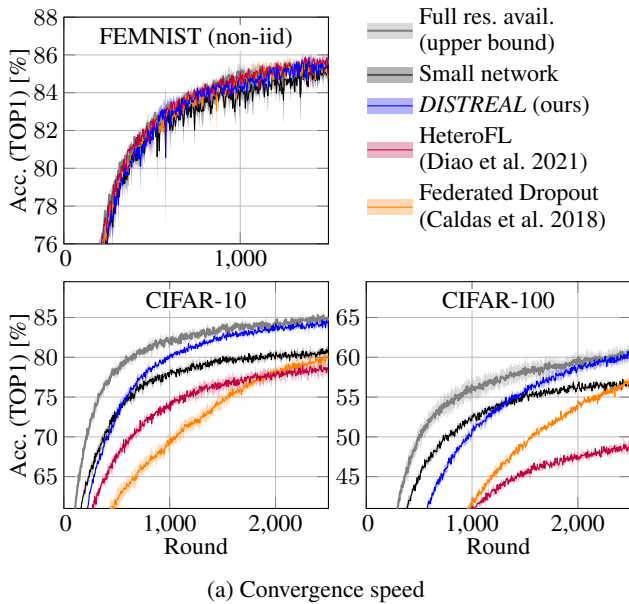
i5-4570 and an NVIDIA GeForce GTX 980. More details about the NN configurations and the computational complexity of the DSE are presented in the appendix.

We compare *DISTREAL* to four baselines:

1. **Full resource availability.** All devices have the full resources to train the full NN in each round. This is a theoretical baseline, which serves as an upper bound.
2. **Small network.** The NN complexity is reduced to fit the weakest device. Thereby, each device can train the full (reduced) NN in each round with FedAvg. For CIFAR-10 and CIFAR-100, we reduce the depth of DenseNet to 19 and 40, respectively. Because the network of FEMNIST already has only a few layers, we reduce the number of filters of the convolutional layers.
3. **Federated Dropout** as in (Caldas et al. 2018). Similar to our technique, it uses dropout to reduce the computational complexity. However, the same dropout rate is used for all layers. To have a fair comparison, we extend the technique of Caldas et al. (2018) to allow for different dropout rates for different devices according to the resource availability. The rates are determined by the server at the start of each round as in the original technique.
4. **HeteroFL** as in (Diao, Ding, and Tarokh 2021). It uses a shrinking ratio $0 < s < 1$. The NN is divided into several levels $p = 1, 2, \dots$, where level p reduces the width of each hidden channel to a fraction s^{p-1} . This is done on the server at the beginning of each round. (Diao, Ding, and Tarokh 2021) provides no details on how to set s . We use $s=0.7$, as it shows the best performance.

Heterogeneity Across Devices We first study heterogeneity across devices, i.e., devices have different resource availability but for now, there are no changes over time. We select the resource availability at each device randomly and uniformly from a range with the upper bound being selected such that training the full NN without dropout is possible. The variability in the resource availability, i.e., ratio of upper to lower bound in the range, is reported in Table 1. We repeat every experiment three times and report the average and standard deviations of the classification accuracy.

Fig. 5 shows the accuracy results for the three datasets. FEMNIST uses a simple network. We observe that the small network baseline has the lowest convergence speed, with all other techniques showing similar performance. The varying quantity (see Table 1) and distribution of local data on the devices make the training noisy. Nevertheless, *DISTREAL* is not more sensitive to non-iid data than other solutions and reaches the same convergence speed and final accuracy. With CIFAR-10, *DISTREAL* achieves a significantly higher convergence speed than Federated Dropout or HeteroFL and reaches the accuracy of the theoretical baseline after 2,000 rounds. The simple baseline that uses a smaller network on all devices initially converges faster but saturates early. We also evaluate the final accuracy, where we train with each technique for 7,500 rounds. This ensures that all techniques have fully converged. *DISTREAL* and Federated Dropout reach the highest final accuracy, similar to the upper bound of full resource availability. Similar observations



(a) Convergence speed

	FEMNIST	CIFAR-10	CIFAR-100
Full res. avail. (upper bound)	87.4±0.3	87.8±0.1	65.6±0.5
Small NN	86.4±0.1	82.2±0.6	57.8±0.5
DISTREAL	86.7±0.1	85.7±0.3	65.7±0.5
Diao 2021	<u>87.1±0.4</u>	81.2±0.5	52.2±0.6
Caldas 2018	86.9±0.3	84.2±0.3	65.3±0.5

(b) Final accuracy (after 7,500 rounds)

Figure 5: Convergence during FL on heterogeneous devices. *DISTREAL* improves the convergence speed, while still reaching the same or a higher final accuracy than others.

can be made with CIFAR-100.

As the resources are not changing over time, the main contributions of *DISTREAL* in this scenario are the application of the DSE, which enable devices to efficiently utilize the available resources and the fact that *DISTREAL* applies a probabilistic approach and drops different filters in different mini-batches, allowing to support a large number of resource levels. It, therefore, outperforms Federated Dropout in terms of convergence speed, which uses the same dropout rates over all the layers, and HeteroFL, which supports only a few resource levels and removes the filters in always the same order, as *DISTREAL* fully utilizes the available resources, and uses these resources more efficiently w.r.t. convergence. Besides, deeper is the trained model, higher is the relative gain.

Heterogeneity Across Devices and Over Time This section studies a fully heterogeneous FL system, i.e., resource availability varies between devices and for each device over time. As discussed in the introduction, this for instance due to shared resource contention between the learning task and other tasks. The available resources for learning may change at any time (workload changes happen in the order of seconds (Tu et al. 2014)), i.e., also in the middle of a round.

As these changes stem from changes in the environment, they may be unpredictable to the device (Duc et al. 2019). We model them as random, with the time between changes following an exponential distribution with rate parameter λ . The absolute resource availability levels are sampled from the same range as in the previous section, i.e., also according to Table 1. Thereby, the average resource availability across all devices and over time is the same as in the previous section. We study four different values of $\lambda \in \{0.5, 1, 2, 4\}$, to simulate a range of slowly to rapidly changing scenarios.

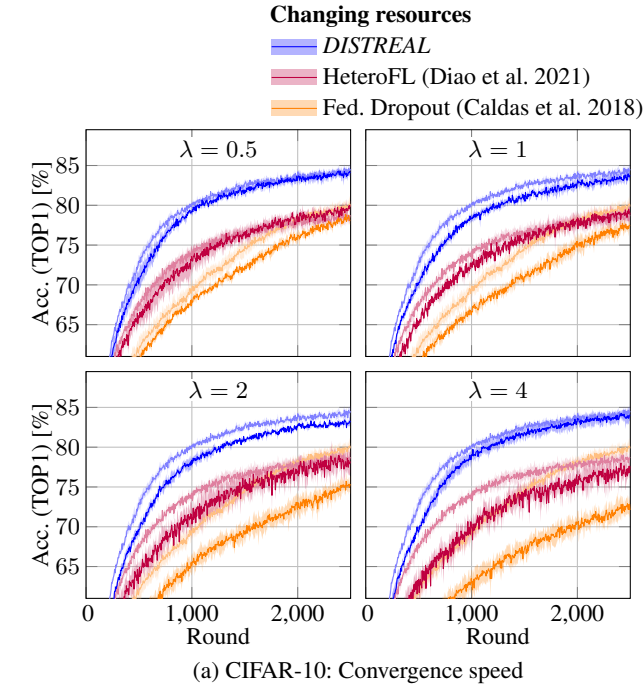
Figs. 6a and 6b show the convergence speed for CIFAR-10 and CIFAR-100, respectively. We also plot the convergence speed with constant resources (previous results from Fig. 5a) for reference. We observe that for both datasets, the convergence speed with *DISTREAL* is not dependent on the rate of resource changes and almost matches the results of the previous section. In contrast, the convergence speeds of HeteroFL and Federated Dropout significantly degrade with higher λ . In addition, *DISTREAL* reaches the highest final accuracy (Figs. 6c and 6d), independently of λ . The baselines with full resource availability and small model perform the same as in Fig. 5, therefore are not shown again.

HeteroFL and Federated Dropout both select the trained model subsets on devices at the server at the start of a round. The devices train on the assigned subset for the whole round and hence cannot react to potential unpredictable changes in the resource availability during a round. An increase in resource availability results in underutilization of available resources, as training finishes early and the device is idle until the end of the round. A decrease in resource availability results in the training not finishing in time (i.e., the device becomes a straggler), leading to the device being dropped from the round. In contrast, *DISTREAL* adjusts the resource requirements of training at run time by selecting a different dropout vector when a change occurs, finishing the training in time and fully utilizing the available resources.

These results show the importance of tackling the challenges discussed in the introduction, to *fully* and *efficiently* utilize available resources on each device. Our technique achieves this by performing dropout at the devices, enabling them to react fast to the changes in a fine-grained manner. This enables to fully utilize all available resources, making convergence robust to changes in the resource availability. Furthermore, the DSE enables us to efficiently utilize the available resources by finding Pareto-optimal dropout vectors w.r.t. resource requirements and achieved convergence speed. These gains in convergence speed do not come at the cost of a lower final accuracy.

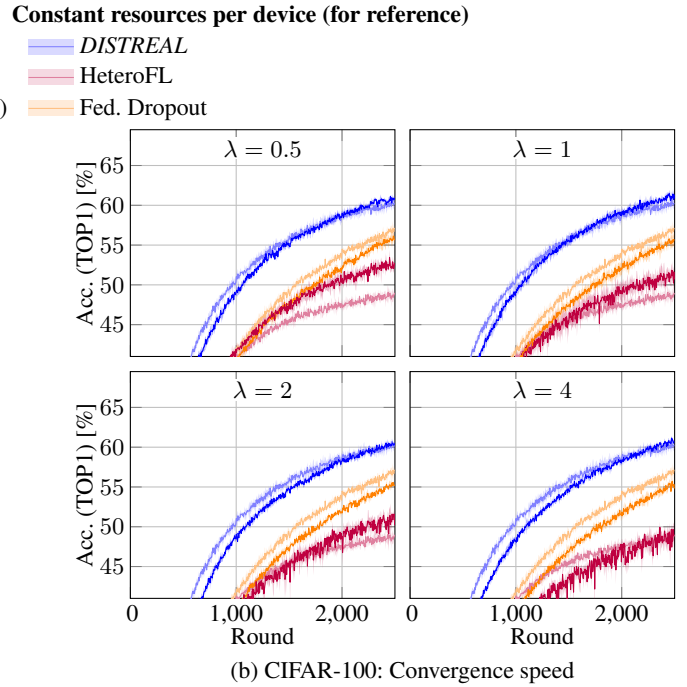
Conclusion

We addressed the problem of distributed training of NNs under heterogeneous resource availability, proposing *DISTREAL*. Our results show that *DISTREAL* significantly improves the convergence speed in a heterogeneous FL system, where resources vary both between devices *and over time* without compromising on the final accuracy. This is as our solution provides each device the capability to adjust the training in a fine-grained manner, enabling it to fully and efficiently utilize its available, but limited, resources.



	$\lambda = 0.5$	$\lambda = 1$	$\lambda = 2$	$\lambda = 4$
<i>DISTREAL</i>	86.3 ± 0.3	86.0 ± 0.2	85.1 ± 0.3	85.9 ± 0.4
Diao 2021	82.6 ± 0.2	81.9 ± 1.3	81.7 ± 0.5	81.3 ± 0.3
Caldas 2018	83.4 ± 0.6	83.2 ± 0.4	82.4 ± 0.4	82.7 ± 0.6

(c) CIFAR-10: Final accuracy (after 7,500 rounds)



	$\lambda = 0.5$	$\lambda = 1$	$\lambda = 2$	$\lambda = 4$
<i>DISTREAL</i>	65.4 ± 0.4	65.5 ± 0.9	64.7 ± 0.3	64.7 ± 0.3
Diao 2021	57.2 ± 0.4	56.8 ± 1.0	56.5 ± 1.0	56.6 ± 1.0
Caldas 2018	65.0 ± 0.3	64.5 ± 0.2	64.5 ± 0.3	64.5 ± 0.3

(d) CIFAR-100: Final accuracy (after 7,500 rounds)

Figure 6: Convergence with CIFAR-10 and CIFAR-100 on heterogeneous devices where resources availability changes randomly over the time with varying rate parameter λ . *DISTREAL* achieves a higher convergence speed than the state of the art, and the highest final accuracy, independently of λ . Experiments with full resource availability or with a small network are not repeated as they perform the same as in Fig. 5.

Acknowledgments

This work is in parts funded by the Deutsches Bundesministerium für Bildung und Forschung (BMBF, Federal Ministry of Education and Research in Germany).

References

- Abadi, M.; Agarwal, A.; Barham, P.; Brevdo, E.; Chen, Z.; Citro, C.; Corrado, G. S.; Davis, A.; Dean, J.; Devin, M.; Ghemawat, S.; Goodfellow, I.; Harp, A.; Irving, G.; Isard, M.; Jia, Y.; Jozefowicz, R.; Kaiser, L.; Kudlur, M.; Levenberg, J.; Mané, D.; Monga, R.; Moore, S.; Murray, D.; Olah, C.; Schuster, M.; Shlens, J.; Steiner, B.; Sutskever, I.; Talwar, K.; Tucker, P.; Vanhoucke, V.; Vasudevan, V.; Viégas, F.; Vinyals, O.; Warden, P.; Wattenberg, M.; Wicke, M.; Yu, Y.; and Zheng, X. 2015. TensorFlow: Large-Scale Machine Learning on Heterogeneous Systems.
- Amir, M.; and Givargis, T. 2018. Priority Neuron: A Resource-Aware Neural Network for Cyber-Physical Systems. *Transactions on Computer-Aided Design of Integrated Circuits and Systems (TCAD)*, 37(11): 2732–2742.
- Amodei, D.; Hernandez, D.; Sastry, G.; Clark, J.; Brockman, G.; and Sutskever, I. 2018. AI and Compute. <https://openai.com/blog/ai-and-compute/>. Accessed: 2020-09-29.
- Ananthanarayanan, G.; Bahl, P.; Bodík, P.; Chintalapudi, K.; Philipose, M.; Ravindranath, L.; and Sinha, S. 2017. Real-Time Video Analytics: The Killer App for Edge Computing. *Computer*, 50(10): 58–67.
- Baker, B.; Gupta, O.; Raskar, R.; and Naik, N. 2017. Accelerating Neural Architecture Search using Performance Prediction. *arXiv preprint arXiv:1705.10823*.
- Bernardos, C. J.; and Uusitalo, M. A. 2021. European Vision for the 6G Network Ecosystem.
- Biscani, F.; and Izzo, D. 2020. A Parallel Global Multiobjective Framework for Optimization: pagmo. *Journal of Open Source Software*, 5(53): 2338.
- Bonawitz, K.; Eichner, H.; Grieskamp, W.; Huba, D.; Ingerman, A.; Ivanov, V.; Kiddon, C.; Konečný, J.; Mazzocchi, S.; McMahan, H. B.; Overveldt, T. V.; Petrou, D.; Ramage, D.; and Roselander, J. 2019. Towards Federated Learning at Scale: System Design. In *SysML Conference*.
- Caldas, S.; Duddu, S. M. K.; Wu, P.; Li, T.; Konečný, J.; McMahan, H. B.; Smith, V.; and Talwalkar, A. 2019. Leaf: A

- benchmark for federated settings. In *Conference on Neural Information Processing Systems (NeurIPS)*.
- Caldas, S.; Konečný, J.; McMahan, H. B.; and Talwalkar, A. 2018. Expanding the Reach of Federated Learning by Reducing Client Resource Requirements. *arXiv preprint arXiv:1812.07210*.
- Chang, H.; Shejwalkar, V.; Shokri, R.; and Houmansadr, A. 2019. Cronus: Robust and Heterogeneous Collaborative Learning with Black-Box Knowledge Transfer. *arXiv preprint arXiv:1912.11279*.
- Chen, Y.; Ning, Y.; Slawski, M.; and Rangwala, H. 2020a. Asynchronous Online Federated Learning for Edge Devices with Non-IID Data. In *International Conference on Big Data (Big Data)*. IEEE.
- Chen, Y.; Qin, X.; Wang, J.; Yu, C.; and Gao, W. 2020b. FedHealth: A Federated Transfer Learning Framework for Wearable Healthcare. *IEEE Intelligent Systems*, 35(4).
- Chen, Y.; Xie, Y.; Song, L.; Chen, F.; and Tang, T. 2020c. A Survey of Accelerator Architectures for Deep Neural Networks. *Engineering*, 6(3): 264–274.
- Cohen, G.; Afshar, S.; Tapson, J.; and Van Schaik, A. 2017. EMNIST: Extending MNIST to Handwritten Letters. In *International Joint Conference on Neural Networks (IJCNN)*.
- Deb, K.; Pratap, A.; Agarwal, S.; and Meyarivan, T. 2002. A Fast and Elitist Multiobjective Genetic Algorithm: NSGA-II. *IEEE Transactions on Evolutionary Computation*, 6(2): 182–197.
- Dhar, S.; Guo, J.; Liu, J.; Tripathi, S.; Kurup, U.; and Shah, M. 2019. On-device Machine Learning: An Algorithms and Learning Theory Perspective. *arXiv preprint arXiv:1911.00623*.
- Diao, E.; Ding, J.; and Tarokh, V. 2021. HeteroFL: Computation and Communication Efficient Federated Learning for Heterogeneous Clients. In *International Conference on Learning Representations (ICLR)*. IEEE.
- Duc, T. L.; Leiva, R. G.; Casari, P.; and Östberg, P.-O. 2019. Machine Learning Methods for Reliable Resource Provisioning in Edge-Cloud Computing: A Survey. *ACM Computing Surveys (CSUR)*, 52(5).
- Elsken, T.; Metzen, J. H.; and Hutter, F. 2019. Neural Architecture Search: A Survey. *Journal of Machine Learning Research (JMLR)*, 20.
- European Commission. 2021a. HORIZON-CL4-2022-DATA-01-02 – Cognitive Cloud: AI-enabled Computing Continuum from Cloud to Edge (RIA).
- European Commission. 2021b. HORIZON-CL4-2022-DATA-01-03 – Programming Tools For Decentralised Intelligence and Swarms (RIA).
- Graham, B.; Reizenstein, J.; and Robinson, L. 2015. Efficient Batchwise Dropout Training using Submatrices. *arXiv preprint arXiv:1502.02478*.
- Horváth, S.; Laskaridis, S.; Almeida, M.; Leontiadis, I.; Venieris, S. I.; and Lane, N. D. 2021. FjORD: Fair and Accurate Federated Learning under heterogeneous targets with Ordered Dropout. *arXiv preprint arXiv:2102.13451*.
- Howard, A. G.; Zhu, M.; Chen, B.; Kalenichenko, D.; Wang, W.; Weyand, T.; Andreetto, M.; and Adam, H. 2017. MobileNets: Efficient Convolutional Neural Networks for Mobile Vision Applications. *arXiv preprint arXiv:1704.04861*.
- Huang, G.; Liu, Z.; Van Der Maaten, L.; and Weinberger, K. Q. 2017. Densely Connected Convolutional Networks. In *Conference on Computer Vision and Pattern Recognition (CVPR)*.
- Huang, G.; Sun, Y.; Liu, Z.; Sedra, D.; and Weinberger, K. Q. 2016. Deep Networks with Stochastic Depth. In *European Conference on Computer Vision (ECCV)*. Springer.
- Imteaj, A.; Thakker, U.; Wang, S.; Li, J.; and Amini, M. H. 2020. Federated Learning for Resource-Constrained IoT Devices: Panoramas and State-of-the-art. *arXiv preprint arXiv:2002.10610*.
- Krizhevsky, A.; and Hinton, G. 2009. Learning Multiple Layers of Features from Tiny Images. *University of Toronto*.
- Krizhevsky, A.; Sutskever, I.; and Hinton, G. E. 2012. ImageNet Classification with Deep Convolutional Neural Networks. In *Neural Information Processing Systems (NIPS)*.
- Li, C.; Wang, G.; Wang, B.; Liang, X.; Li, Z.; and Chang, X. 2021a. Dynamic Slimmable Network. In *Conference on Computer Vision and Pattern Recognition (CVPR)*.
- Li, C.; Yu, Z.; Fu, Y.; Zhang, Y.; Zhao, Y.; You, H.; Yu, Q.; Wang, Y.; and Lin, Y. 2021b. HW-NAS-Bench: Hardware-Aware Neural Architecture Search Benchmark. *International Conference on Learning Representations (ICLR)*.
- Li, D.; and Wang, J. 2019. Fedmd: Heterogeneous Federated Learning via Model Distillation. In *Conference on Neural Information Processing Systems (NeurIPS)*.
- Li, T.; Sahu, A. K.; Talwalkar, A.; and Smith, V. 2020a. Federated Learning: Challenges, Methods, and Future Directions. *IEEE Signal Processing Magazine*, 37(3): 50–60.
- Li, T.; Sahu, A. K.; Zaheer, M.; Sanjabi, M.; Talwalkar, A.; and Smith, V. 2020b. Federated Optimization in Heterogeneous Networks. In *Machine Learning and Systems (MLSys)*, volume 2.
- Lin, T.; Kong, L.; Stich, S. U.; and Jaggi, M. 2020. Ensemble Distillation for Robust Model Fusion in Federated Learning. In *Conference on Neural Information Processing Systems (NeurIPS)*.
- Liu, B.; Wang, L.; and Liu, M. 2019. Lifelong Federated Reinforcement Learning: A Learning Architecture for Navigation in Cloud Robotic Systems. *IEEE Robotics and Automation Letters*, 4(4): 4555–4562.
- McMahan, H. B.; Moore, E.; Ramage, D.; Hampson, S.; et al. 2017. Communication-Efficient Learning of Deep Networks from Decentralized Data. In *International Conference on Artificial Intelligence and Statistics (AISTATS)*.
- Mnih, V.; Badia, A. P.; Mirza, M.; Graves, A.; Lillicrap, T.; Harley, T.; Silver, D.; and Kavukcuoglu, K. 2016. Asynchronous Methods for Deep Reinforcement Learning. In *International Conference on Machine Learning (ICML)*.
- NetWorld. 2020. Smart Networks in the Context of NGI.

- Paszke, A.; Gross, S.; Massa, F.; Lerer, A.; Bradbury, J.; Chanan, G.; Killeen, T.; Lin, Z.; Gimelshein, N.; Antiga, L.; Desmaison, A.; Kopf, A.; Yang, E.; DeVito, Z.; Raison, M.; Tejani, A.; Chilamkurthy, S.; Steiner, B.; Fang, L.; Bai, J.; and Chintala, S. 2019. PyTorch: An Imperative Style, High-Performance Deep Learning Library. In *Neural Information Processing Systems (NeurIPS)*, 8024–8035.
- Rapp, M.; Khalili, R.; and Henkel, J. 2020. Distributed Learning on Heterogeneous Resource-Constrained Devices. *arXiv preprint arXiv:2006.05403*.
- Shi, Y.; Yang, K.; Jiang, T.; Zhang, J.; and Letaief, K. B. 2020. Communication-Efficient Edge AI: Algorithms and Systems. *IEEE Communications Surveys & Tutorials*, 22(4).
- Silver, D.; Huang, A.; Maddison, C. J.; Guez, A.; Sifre, L.; van den Driessche, G.; Schrittwieser, J.; Antonoglou, I.; Panneershelvam, V.; Lanctot, M.; Dieleman, S.; Grewe, D.; Nham, J.; Kalchbrenner, N.; Sutskever, I.; Lillicrap, T. P.; Leach, M.; Kavukcuoglu, K.; Graepel, T.; and Hassabis, D. 2016. Mastering the Game of Go with Deep Neural Networks and Tree Search. *Nature*, 529(7587): 484–489.
- Song, Z.; Wang, R.; Ru, D.; Peng, Z.; Huang, H.; Zhao, H.; Liang, X.; and Jiang, L. 2019. Approximate Random Dropout for DNN Training Acceleration in GPGPU. In *Design, Automation & Test in Europe Conference & Exhibition (DATE)*. IEEE.
- Srivastava, N.; Hinton, G.; Krizhevsky, A.; Sutskever, I.; and Salakhutdinov, R. 2014. Dropout: a Simple Way to Prevent Neural Networks from Overfitting. *Journal of Machine Learning Research (JMLR)*, 15(1): 1929–1958.
- Tan, M.; and Le, Q. 2019. EfficientNet: Rethinking Model Scaling for Convolutional Neural Networks. In *International Conference on Machine Learning (ICML)*.
- Tann, H.; Hashemi, S.; Bahar, R. I.; and Reda, S. 2016. Runtime Configurable Deep Neural Networks for Energy-Accuracy Trade-Off. In *Int. Conf. on Hardware/Software Codesign and System Synthesis (CODES+ISSS)*. IEEE.
- Thakker, U.; Beu, J.; Gope, D.; Zhou, C.; Fedorov, I.; Dasika, G.; and Mattina, M. 2019. Compressing RNNs for IoT Devices by 15-38x using Kronecker Products. *arXiv preprint arXiv:1906.02876*.
- Tu, C.-H.; Hsu, H.-H.; Chen, J.-H.; Chen, C.-H.; and Hung, S.-H. 2014. Performance and Power Profiling for Emulated Android Systems. *ACM Transactions on Design Automation of Electronic Systems (TODAES)*, 19(2).
- Xie, C.; Koyejo, S.; and Gupta, I. 2020. Asynchronous Federated Optimization. In *Workshop on Optimization for Machine Learning*.
- Xu, Z.; Yang, Z.; Xiong, J.; Yang, J.; and Chen, X. 2019. ELFISH: Resource-Aware Federated Learning on Heterogeneous Edge Devices. *arXiv preprint arXiv:1912.01684*.
- Yang, T.; Andrew, G.; Eichner, H.; Sun, H.; Li, W.; Kong, N.; Ramage, D.; and Beaufays, F. 2018. Applied Federated Learning: Improving Google Keyboard Query Suggestions. *arXiv preprint arXiv:1812.02903*.
- You, Y.; Zhang, Z.; Hsieh, C.-J.; Demmel, J.; and Keutzer, K. 2018. ImageNet Training in Minutes. In *International Conference on Parallel Processing (ICPP)*.
- Yu, J.; Yang, L.; Xu, N.; Yang, J.; and Huang, T. 2018. Slimmable Neural Networks. *International Conference on Learning Representations (ICLR)*.
- Yu, R.; and Li, P. 2021. Toward Resource-Efficient Federated Learning in Mobile Edge Computing. *IEEE Network*, 35(1): 148–155.
- Zhang, C.; Patras, P.; and Haddadi, H. 2019. Deep Learning in Mobile and Wireless Networking: A Survey. *IEEE Communications Surveys and Tutorials*, 21(3): 2224–2287.
- Zhang, H.; Ananthanarayanan, G.; Bodik, P.; Philipose, M.; Bahl, P.; and Freedman, M. J. 2017. Live Video Analytics at Scale With Approximation and Delay-Tolerance. In *USENIX Symposium on Networked Systems Design and Implementation (NSDI)*.
- Zhou, Z.; Chen, X.; Li, E.; Zeng, L.; Luo, K.; and Zhang, J. 2019. Edge Intelligence: Paving the Last Mile of Artificial Intelligence with Edge Computing. *Proceedings of the IEEE*, 107(8): 1738–1762.

Structured Dropout

This section provides more details of filter-based structured dropout that is used to reduce the required resources (amount of computation) for training.

Number of MACs

Structured dropout is a probabilistic process, i.e., a different number of filters may be dropped in every mini-batch. Table 2 shows for the most important layers in a convolutional neural network (CNN) how the *expected* number of MACs in the forward pass depends on the dropout rate. For a convolutional layer, it depends not only on the dropout rate of this layer but also on the dropout rate of the preceding convolutional layer because a reduced number of filters (dropout of this layer) is applied to a reduced number of input feature maps (previous layer). In the specific case that all per-layer dropout rates are the same, the expected number of MACs reduces quadratically with the dropout rate. Most other layers (batch normalization, activation, pooling) operate on each feature map independently. Their expected number of MACs scales linearly with the dropout rate.

Resource Requirements and Availability

Structured dropout reduces the theoretical amount of computation, i.e., the number of MACs. This also affects the resource requirements of training, which can be measured in many ways: execution time, energy, etc. We study in this section the relationship between the theoretical amount of computation and the resource requirements and show that

1. MACs are a correct abstraction, i.e., they strongly correlate with the underlying resource.
2. MACs are a practical abstraction, i.e., it is possible to determine the available MACs/s at run time.

We pick the execution time of training on the CPU of a Raspberry Pi 4 with 2 GB RAM as an example. The implementation is done in 32-bit PyTorch 1.7.1.

For the first point, we measure the execution time of one mini-batch (size 128) of training DenseNet-40 with each

Layer Type	MACs
Convolution	$(1-d) \cdot Y \cdot ((1-d_p) \cdot c_i \cdot k_w \cdot k_h + b)$ where
	d dropout rate in this layer
	$ Y $ nb. of output pixels
	d_p dropout rate in the prev. layer
	c_i input channels
	k_w, k_h kernel width and height
	b 1 if bias is used, 0 otherwise
Batch Norm., Activation, Pooling	$(1 - d_p) \cdot x$ where
	d_p dropout rate in the prev. layer
	x nb. of MACs w/o dropout

Table 2: Expected number of MACs of the forward pass of individual layers with structured dropout.

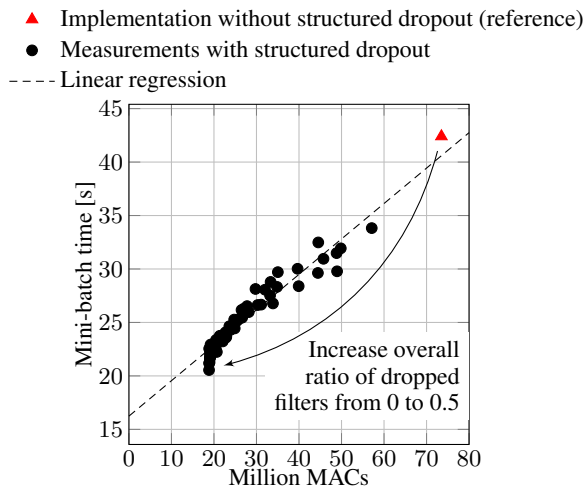


Figure 7: Mini-batch training time of DenseNet-40 for different dropout vectors on a Raspberry Pi 4 shows a linear relationship with the number of MACs in the forward pass.

dropout vectors found by the DSE. Fig. 7 plots the execution time (forward and backward pass) over the number of MACs in the forward pass. We make two main observations. Firstly, the execution time is significantly reduced compared to an implementation of the same NN without any dropout, i.e., with vanilla PyTorch layers. This demonstrates the suitability to employ structured dropout to reduce the resource requirements (CPU time). We observe that the copy overheads depend on the underlying architecture. On platforms with separate VRAM for the GPU, copy overheads are higher. An implementation revision is required to obtain similar benefits as on platforms with shared memory between CPU and GPU. Because we target distributed devices, such as IoT devices that have a shared memory for CPU and GPU or even perform training on the CPU, this is a topic of future work. Secondly, the mini-batch training time shows a clear linear relationship with the number of MACs. Consequently, the number of MACs in the forward pass is a good approximation of the actual resource requirements during training, and can be used in the DSE to determine the fitness of a dropout vector. A constant offset has no impact, as the fitness is normalized to $[0, 1]$.

Note that in a general case, estimating the resource requirements from the total number of MAC may be inaccurate (Li et al. 2021b). This comes from the fact that different layer types may result in a different relationship between resource requirements and the theoretical number of MACs. This is for example the case if different layers cause different data movement between the main memory and the CPU, or if different layers can be accelerated differently by vectorization. However, *we use the number of MACs only to compare different configurations (dropout vectors) of the same topology, i.e., we do not compare different topologies.* Therefore, the number of MACs is closely related to the resource requirements.

Due to this close correlation with the training time, the

number of available MACs for training can also be derived at run time. As an example, we consider the CPU time as the limited resource due to resource contention. In this example, the FL training is one of several tasks that are executed on the system, and that compete for CPU time. The operating system scheduler decides the time during which each application is executed on the system based on many factors, such as fairness or priorities. The amount of CPU time available for training is, therefore, known at the OS level and is made available to the application. From the CPU time and desired throughput, one can directly obtain the time per mini-batch. Finally, the number of MACs can be derived from the mini-batch training time as in Fig. 7. This shows the practicality of such abstraction, proving the second point.

Implementation in PyTorch

This section summarizes our implementation of dropout in PyTorch, which is publicly available⁴.

Convolutional layers A convolutional layer performs the following computation:

$$O = I * W + B, \quad (2)$$

where $O \in \mathbb{R}^{b \times c_o \times w_o \times h_o}$ is the output activation (b samples per mini-batch, c_o output feature maps, width w_o and height h_o of the output feature maps), $I \in \mathbb{R}^{b \times c_i \times w_i \times h_i}$ is the input activation (c_i input feature maps, width w_i and height h_i of the input feature maps), $W \in \mathbb{R}^{c_o \times c_i \times k_w \times k_h}$ (width k_w and height k_h of the convolutional kernel) and $B \in \mathbb{R}^{c_o}$ are the weights and bias.

Structured dropout drops some of the filters from the computation, i.e., some of the feature maps in O are replaced by 0. Dropout in a preceding layer results in some of the input feature maps to contain only 0. To benefit from dropout in terms of computational requirements, unnecessary computations need to be avoided. This is achieved by excluding dropped parts from the computations by performing sparse convolution.

Let V_i denote the set of the indices of valid (not dropped) feature maps in the input I of the convolutional layer. V_o is the set of the indices of valid feature maps in the output O and is obtained from a Bernoulli process with the dropout rate d . $O' \in \mathbb{R}^{b \times |V_o| \times w_o \times h_o}$ represents the valid output feature maps in O , $I' \in \mathbb{R}^{b \times |V_i| \times w_i \times h_i}$ represents the valid input feature maps in I . It follows that

$$O' = I' * W[V_o, V_i, :, :] + B[V_o], \quad (3)$$

where $W[V_o, V_i, :, :]$ represents the parts of W that are obtained by keeping only valid columns/rows according to V_o and V_i (same for $B[V_o]$). The sparse convolution can be replaced by a regular (dense) convolution on the subsampled inputs. This subsampling of W and B needs to be done at run time in every mini-batch because V_i and V_o may change in every mini-batch. However, if the following layer is aware of V_o , the output O does not need to be reconstructed from O' , and O' can be forwarded to the next layer unchanged.

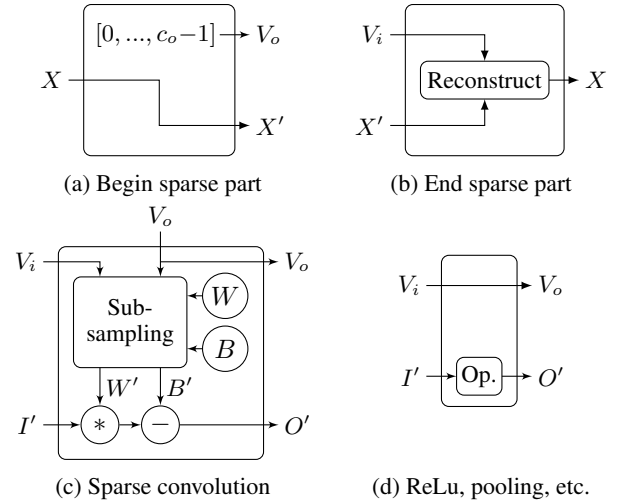


Figure 8: Building blocks for sparse NN that results from filter-based structured dropout.

Our implementation avoids copying input and output activations. This is achieved by operating on sparse representations of O and I instead. These are tuples (O', V_o) and (I', V_i) . However, this requires implementing a custom convolutional layer to manage the sparse computations. Fig. 8c depicts a sparse convolutional layer for structured dropout with rate d .

PyTorch stores weight and activations in tensors, i.e., multi-dimensional matrices. Tensors in PyTorch are regular, i.e., they store data in memory with fixed strides. Subsampling the weights W and B according to V_i and V_o would result in irregular stride pattern, and therefore requires copying the underlying data in memory. This could be avoided by extending the backend to be aware of V_i and V_o , and still providing the full W and B to the backend. However, PyTorch supports several backends, some of which (e.g., CUDA) comprise proprietary code, and cannot be modified easily. It is also important to notice that the weight and bias tensors in convolutional layers are much smaller than the input and output activation, lowering the copy overheads.

Dropout Traditional dropout performs two operations during training: it replaces dropped values by 0 and scales non-dropped values by $1/(1 - d)$. In our implementation of structured dropout, these two operations need to be separated. The first operation is performed by passing the indices of feature maps to compute V_o to the preceding convolutional layer. Scaling needs to be done at a later step, potentially with other layers (like batch normalization) in between.

Other layers Many layers, such as activation, pooling, etc. operate on individual feature maps independently. As a result, these operations can directly be applied to the valid feature maps I' . The indices of the valid feature maps of the output of this operation V_o are the same as of the input V_i , as depicted in Fig. 8d. We require two additional layers that begin and end the sparse part of the NN, respectively. The begin layer (Fig. 8a) annotates the activation with the infor-

⁴<https://git.scc.kit.edu/CES/DISTREAL>

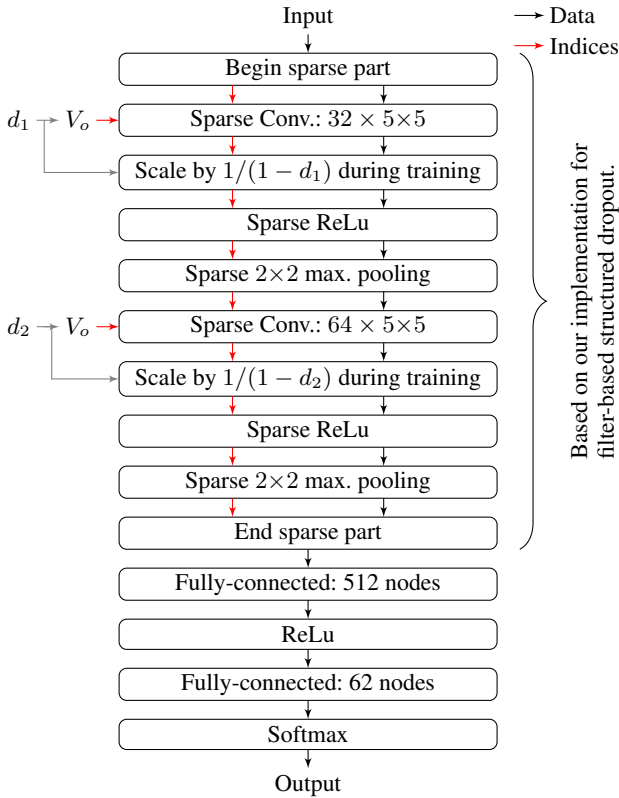


Figure 9: NN for FEMNIST with sparse computations resulting from filter-based structured dropout.

mation that all feature maps are valid ($V_o = [1, \dots, c_o - 1]$). This does not require any copy. The end layer (Fig. 8b) fills in zeros at the positions of invalid feature maps. This requires copying tensors. However, this layer is only required once. We did not implement sparse fully-connected layers but similar concepts as for the convolutional layers can be applied.

Fig. 9 illustrates how these sparse layers can be used in a whole NN that consists of a sparse convolutional part and a dense fully-connected part.

Experimental Details

DSE

This section provides details on how our DSE employs the NSGA-II evolutionary algorithm from pygmo2 (Biscani and Izzo 2020).

NSGA-II Parameters We use the default parameters provided in pygmo2, i.e., the crossover probability is set at 0.95, the distribution index for crossover is set at 10, the mutation probability is set at 0.01, and the distribution index for mutation is set at 50. The population size is 64. The size of individuals is 2, 39, and 99 continuous per-layer dropout rates for the networks used with FEMNIST, CIFAR-10 (DenseNet-40), and CIFAR-100 (DenseNet-100), respectively. The minimum and maximum dropout rates are set at 0 and 0.5, respectively.

Initial Population The initial population comprises 62 random individuals (dropout rates sampled randomly from $[0, 0.5]$). We add two individuals with dropout rates set at all 0 or all 0.5 to accelerate the exploration of the Pareto-front.

Fitness Evaluation To evolve the population by one generation, first the fitness of each individual is assessed. The resource requirements are the expected number of MACs according to the equations in Table 2. As explained in the section on resource-aware training, the convergence speed is measured by observing the accuracy change after short training. This short training comprises 64 mini-batches of size 64. The optimizer is stochastic gradient descent (SGD) with momentum set at 0.9 and weight decay of 10^{-4} . The learning rates are set at 0.005 for the network with FEMNIST, and 0.01 for DenseNet-40/100. The training starts from a snapshot that has been pre-trained on a distorted dataset. For CIFAR-10/100, this distortion changes the brightness, contrast, saturation and hue by 0.5 using PyTorch `ColorJitter` class. For the grayscale FEMNIST, we rotate images by 90 degrees. Training is repeated with three random seeds (used both for pre-training and short training) to obtain an average accuracy improvement. Fitness values are normalized according to Eq. (1).

Miscellaneous Training Parameters

This section lists parameters used in the FL experiments that have not been included in the description of the experimental setup. The local training on each device uses mini-batches of size 64. The optimizer is the same as for the fitness evaluation (SGD with momentum set at 0.9 and weight decay of 10^{-4}). The learning rates are set at 0.035 for the network with FEMNIST (as in (Caldas et al. 2018)), and 0.05 for DenseNet-40/100. The NN for FEMNIST is also similar to the one used in (Caldas et al. 2018), i.e., a CNN with two 5×5 convolutional layers with 32 and 64 filters, respectively, each with ReLU activation and each followed by a 2×2 max pooling. The convolutional part is followed by two fully connected layers with 512 and 62 neurons (number of classes), respectively. The implementation of this NN with structured dropout is depicted in Fig. 9. (The NNs for CIFAR-10/100 are explained in the description of the experimental setup.

Compute Time for Experimental Results

We report in this section the compute time required to reproduce our experiments. *These are not the resources that we model on the devices.* We run our experiments on two types of systems. The first type of systems (System 1) runs Ubuntu 18.04.6 LTS and contains an Intel Core i5-4570 with 32 GB RAM and a NVIDIA GeForce GTX 980 with 4 GB VRAM. The second type of systems (System 2) runs CentOS 7.9.2009 and contains an AMD Ryzen 7 2700X with 64 GB RAM and no GPU. We report the total compute time without considering parallelization to several machines.

Table 3 shows the compute time for our DSE, which runs only once at design time. Compute times report the total compute if run on *either* of the two systems. Different networks require different numbers of generations to converge.

Dataset	NN	Generations	Total compute time	
			System 1	or System 2
FEMNIST	Conv. NN	20	15 h	5.5 h
CIFAR-10	Densenet-40	50	270 h	170 h
CIFAR-100	Densenet-100	50	330 h	480 h

Table 3: Compute time to run the DSE (only once at design time).

Dataset	Resource heterogeneity	Rounds	Experiments	Total compute time	
				System 1	or System 2
FEMNIST	across devices	7,500	5×3	800 h	500 h
CIFAR-10	across devices	7,500	5×3	570 h	1,260 h
CIFAR-100	across devices	7,500	5×3	1,170 h	4,290 h
CIFAR-10	across devices and time	7,500	3×4×3	1,470 h	3,150 h

Table 4: Compute time to reproduce the FL results.

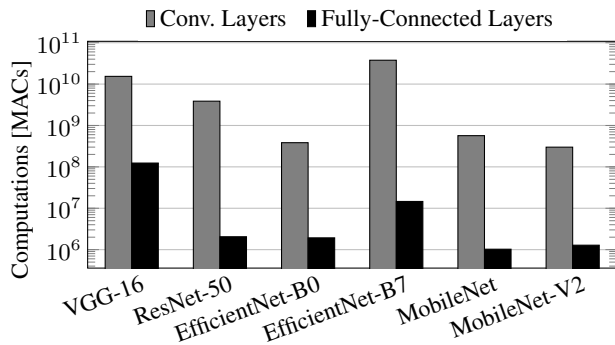


Figure 10: Convolutional layers account for the majority of MAC operations in CNNs.

We use three random seeds to measure the accuracy change after short training for a dropout vector.

Table 4 shows the compute times required to reproduce our experimental results with FL. The number of rounds with the three datasets is reported in Table 4. The experiments with heterogeneity across devices but not over time, each comparing five techniques, are repeated with three random seeds. The experiments with heterogeneity across devices and over time, comparing three techniques in four different rates of change in the resource availability λ , are repeated with three random seeds.

Computations in CNNs

Fig. 10 shows how the number of MACs for the forward pass is distributed between fully-connected and convolutional layer types for different state-of-the-art NNs. We observe that for all architectures, the convolutional part requires orders of magnitude more MACs in total than the fully-connected part.